CERAMICS, MECHANICAL PROPERTIES

1. Introduction

Structural ceramics are used in applications such as gas turbines, advanced heat engines, semiconductor processing equipment, armor, thermal barrier coatings, medical implants, as thin films for wear and electronic applications, heat exchangers, aerospace and weapons components, in high temperature solid oxide fuel cells, and as bearings components. Advantages of ceramics over metals include dimensional stability; low densities, which translate into weight savings and increased fuel efficiencies; high temperature capabilities; and corrosion resistance. Although metals are ductile, and thus have greater damage tolerance than ceramics, the use of metals is limited to much lower temperatures. For example, the melting points of aluminum and 304 stainless steel are 660°C and from 1400–1450°C, respectively, whereas those of alumina, Al_2O_3, and stabilized zirconia are 2020°C and from 2500–2600°C, respectively.

The overriding concern with regard to the mechanical performance of ceramics is their brittleness and, hence, sensitivity to flaws. There is usually little or no warning that failure is imminent because deformation strain prior to failure is usually $<0.1\%$. As a result, a primary thrust of structural ceramics research has been the development of tougher and stronger ceramics. Ceramics are now routinely available that have toughness values of 7–10 $MPa \cdot m^{1/2}$ and strengths that exceed 1000 MPa (1.5×10^5psi) (1) (see also ADVANCED CERAMICS, STRUCTURAL CERAMICS). These values compare to toughness values of 120–153 $MPa \cdot m^{1/2}$ and strengths of 1380–1790 MPa for structural metals such as AF1410 high strength steel (2).

The mechanical properties of ceramics are sensitive to the starting materials, forming processes, heat treatment conditions, and surface preparation. These properties are particularly sensitive to the microstructure, and vary with it in a complex manner. A unique aspect is the dependence of some of the mechanical properties on extremes rather than averages. For example, consider a tensile rod containing a significant volume of pores. In a metal, the remnant cross-sectional area would determine the load-bearing capacity. However, in a ceramic, the stress concentration from a single, large pore could determine the failure stress.

A much more detailed treatment of the mechanical properties of ceramics is available (3).

2. Properties and Behavior

2.1. Elastic Behavior. Elastic deformation is defined as the reversible deformation that occurs when a load is applied. Most ceramics deform in a linear-elastic fashion, ie, the amount of reversible deformation is a linear function of the applied stress up to a certain stress level. If the applied stress is increased any further, the ceramic fractures catastrophically. This is in contrast

Table 1. **Properties of Ceramics and Other Materials**

Material	Young's modulus, GPa[a]	Poisson's ratio
soft rubber	0.007–0.07	0.49
nylon	2.8	0.40
ice	9	0.2–0.88[b]
concrete	14	0.20
aluminum	70	0.34
plate glass	70	0.27
copper	110	0.34
ZrO_2, partially stabilized	205	0.23
Al_2O_3	380	0.26
SiC	207–483	0.14
diamond	1050	0.20

[a] To convert GPa to psi, multiply by 145×10^3.
[b] Values for the Poisson's ratio of ice are highly dependent on composition, structure, and strain rate (4).

to most metals, which initially respond elastically, and then begin to deform plastically. This plastic deformation allows stresses at stress concentrators to be dissipated rather than building to the point where bonds break irreversibly.

Elastic behavior is commonly quantified by the Young's modulus, E, the proportionality constant between the applied tensile stress σ and the tensile strain ε (Δ length/original length).

$$\sigma = E\varepsilon \tag{1}$$

Materials having high elastic moduli deform less for a given stress. Typical E values for several material categories, metals, ceramics, and polymers, are shown in Table 1. As ceramics have mostly covalent and ionic bonding, the bond strengths and consequently the elastic modulus values are high.

Crystals are often anisotropic because bond strengths and density are a function of direction. In single crystals this leads to anisotropy in the elastic moduli such that the strain depends on the stress application direction. Most polycrystalline materials are macroscopically isotropic because the anisotropies of randomly oriented, individual grains (single crystals) average to zero over all the grains. Glasses are elastically isotropic because of a random network structure.

Another commonly used elastic constant is the Poisson's ratio ν, which relates the lateral contraction to longitudinal extension in uniaxial tension. Typical Poisson's ratios are also given in Table 1. Other elastic moduli include the shear modulus G, which describes the amount of strain induced by a shear stress, and the bulk modulus K, which is a proportionality constant between hydrostatic pressure and the negative of the volume change ($-\Delta V/V$).

Porosity has a significant effect on elastic moduli. Empirical relations of the form

$$E = E_o e^{-bP} \tag{2}$$

where E_o = Young's modulus of dense material, P = relative volume of porosity, and b = constant, generally describe the elastic behavior of ceramics. Thermal expansion anisotropy between the various grains comprising a polycrystalline ceramic can result in tensile stresses high enough to produce intergranular cracks, with sizes on the order of the grain size. These cracks, called microcracks, lead to a decrease in the elastic modulus. The grain size of a ceramic has no effect on the modulus unless the material is very anisotropic and contains large grains that microcrack spontaneously.

Young's modulus can be determined by measuring the stress–strain response (static modulus), by measuring the resonant frequency of the body (resonant modulus), or by measuring the velocity of sound through the material (sonic modulus). The values of modulus obtained by static methods are less accurate (within 5–10%) than values using sonic techniques (<1% error).

2.2. Strength. *Measured Strength versus Theoretical Strength.* Strengths of ceramic materials depend both on the types of flaws present and the method of strength measurement. The elastic modulus describes how easily atoms in a solid can be moved together or apart for small deformations (higher values imply the lattice is stiffer). The shape of the interatomic potential is such that beyond a certain spacing, the atomic attraction is insufficient to hold the atoms together. If deformation of the material is continued beyond this point, entire planes of atoms separate and the ceramic fractures.

The theoretical tensile strength of the material, σ_{theor}, has been approximated by

$$\sigma_{theor} = \left(\frac{E\gamma}{a}\right)^{1/2} \approx \frac{E}{10} \tag{3}$$

where a = equilibrium spacing between planes of atoms, γ = fracture surface energy, and E = Young's modulus (5). If all bonds in a material were stressed equally up to the point of failure, the strength of a ceramic would be the theoretical strength. Large discrepancies between the theoretical and measured tensile strengths of ceramics result from the presence of imperfections. These imperfections or flaws can raise the local stress to the point that bonds in the immediate vicinity of the flaw can fail a few at a time, as opposed to every atom in the plane failing simultaneously. Regardless of the shape or orientation of a flaw, the energy required to break bonds in a given material is generally constant.

A flaw such as a simple spherical pore concentrates the stress on the bonds in the vicinity of the pore by a factor of 2 over the applied stress (6); however, most ceramics contain imperfections that enhance the stress to a much greater degree, leading to severe strength reductions. A typical ceramic such as alumina is as much as one hundred times weaker than the theoretical strength.

Stress concentration, such that the crack tip stress exceeds a material's theoretical strength, is a necessary condition for fracture; however, an energy requirement must also be satisfied. It has been recognized that crack growth could only occur if the total energy of the system was lowered by this extension. The energy requirements for crack growth have been postulated to be equal to

the energy required to create two new surfaces. Thus

$$\sigma_{\text{fracture}} = \left(\frac{2E\gamma}{\pi c}\right)^{1/2} \tag{4}$$

where c = crack dimension. The details of this formulation along with extensive information about brittle fracture are available (7).

A more practical approach for quantifying the conditions required for fracture uses a stress intensity criterion instead of an energy criterion. Using linear elastic theory, it has been shown that under an applied stress, σ_{applied}, when the stress intensity, K,

$$K = \sigma_{\text{applied}} Y(c)^{1/2} \tag{5}$$

where Y = flaw and loading geometry factor (8), reached a critical value known as the fracture toughness, K_C, fracture would occur. The applied stress required to cause fracture, σ_{fracture}, can therefore be written as

$$\sigma_{\text{fracture}} = \frac{K_C}{Y(c)^{1/2}} \tag{6}$$

A very large proportion of failures in practical applications of ceramics results from applied tensile stresses. As a consequence, many published tables of properties of ceramic materials contain only tensile strength values. Ceramic strength is typically measured as a bending (flexural) strength because of the difficulties of gripping ceramic samples and achieving pure tension in tensile tests. In flexural tests, the reported strength is the value of the maximum stress at the tensile surface at failure. Guidelines for conducting strength tests are available (9). Measured strengths of ceramics in flexure and compression are shown in Table 2.

Flaws. Pristine, undamaged ceramics (glass fibers and ceramic whiskers) exhibit strengths close to theoretical levels. Strengths of most ceramics, however, seldom approach theoretical levels because of processing flaws and damage introduced by handling, and during service. Examples of flaws commonly found in ceramics are shown in Figure 1.

Although each ceramic has a characteristic theoretical strength, the fracture toughness K_{IC} and the most severe flaw, ie, the flaw that produces the largest stress concentration, normally determine the actual strength. The larger the flaw, the greater the reduction in strength, and flaws in close proximity may act as a single, more severe flaw.

Microstructural effects on strength, such as those from porosity, impurities, grain size, and surface condition, are often difficult to identify because frequently several effects occur simultaneously. A common assumption for the relationship between strength and grain size is that flaw size scales directly with grain size. Hence the strength and grain size, G, are related in a similar manner to strength and flaw size (eq. 6). The strength is

$$\sigma \propto \frac{1}{G^{1/2}} \tag{7}$$

Table 2. **Measured Strengths of Common Ceramics**

Material	Tensile strength			Compressive strength	
	Measurement technique[a]	Value, MPa[b]	Reference	Value, MPa[b]	Reference
soda–lime silica (SLS) glass	ROR	79	10		
chemically strengthened SLS glass	ROR	293	10		
Al_2O_3	FP	370	11	4480	12
SiC	FP	345	13	3680	14
Si_3N_4	FP	1100	1	3450	12
SiAlON	FP	450	15		
SiC reinforced Al_2O_3 composite[c]	FP	640	16		
Y-TZP[d]	TT	745	17		
	FP	1630	17		
ZrO_2, CaO stabilized				2000	12
Al_2O_3/ZrO_2 composite	TP	2400	1		

[a] ROR = ring – on – ring bending; FP = four – point bending; TT = tensile test; and TP = three–point bending.
[b] To convert MPa to psi, multiply by 145.
[c] 30 vol% SiC whisker reinforced.
[d] 2 mol% yttria stabilized tetragonal zirconia polycrystal.

In some cases, it is not the average grain size that determines the strength. For example when exaggerated grain growth results in the formation of a few very large grains in an otherwise fine-grain material, one of those large grains can cause failure. That failure can occur at a stress much lower than expected for the fine-grain structure.

The relation between strength and impurities depends on the location and form of the impurities, and the failure mechanism. If impurities are present as discrete second phases, they can serve as obstacles to crack propagation; however, they can also act as stress concentrators, or as weak grain boundary fracture paths. An indirect effect of impurities on strength relates to their effect on the microstructure, eg, the grain size and shape, and porosity.

Statistical Variation in Strength. The wide variety of flaw types and sizes in ceramics produces the large (typically ±25%) variability in strength that has been one of the principal hurdles to the incorporation of ceramics in structural applications (18). This value compares unfavorably with the few percent for variability of the yield stress of a metal. The failure probability of a ceramic body at a given load depends on the probability of a flaw of a critical size being present in a location where it produces a stress concentration. Some of the strength variability reported in the literature can be attributed to inconsistencies in testing procedures; however, tests performed in accordance with recommended standards can give accurate and consistent results (9,11).

Many distribution functions can be applied to strength data of ceramics. The function that has been most widely applied is the Weibull function, which is based on the concept of failure at the weakest link in a body under simple tension. A normal distribution is inappropriate for ceramic strengths because

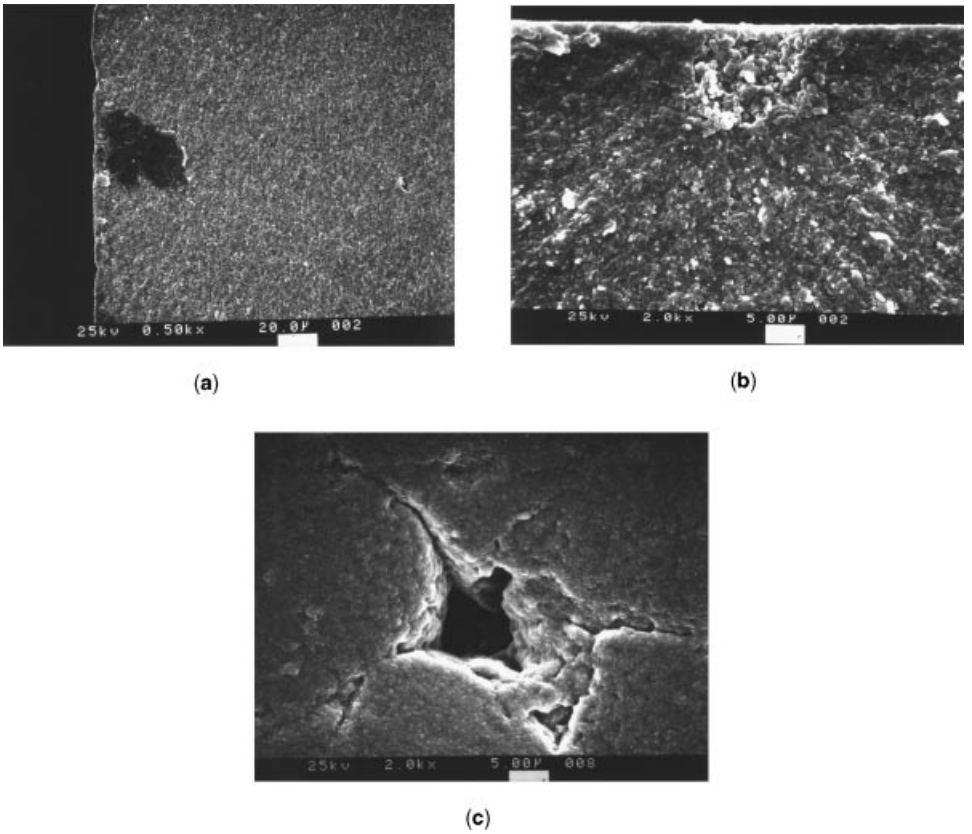

Fig. 1. Strength-reducing flaws commonly found in ceramics: (**a**) large grain surrounded by fine-grain matrix; (**b**) porous region resulting from incomplete densification; and (**c**) pore located where hard powder agglomerates did not sinter together.

extreme values of the flaw distribution, not the central tendency of the flaw distribution, determine the strength. One implication of Weibull statistics is that large bodies are weaker than small bodies because the number of flaws a body contains is proportional to its volume, and the likelihood of finding a large flaw increases with the volume.

The Weibull distribution function expresses the failure probability P_f as a function of the applied stress σ, and three Weibull parameters σ_μ, σ_o, and m

$$P_f = 1 - \exp\left[-\int_V \left(\frac{\sigma - \sigma_\mu}{\sigma_o}\right)^m dV\right] \tag{8}$$

where σ_μ = the threshold stress below which failure does not occur, ie, where $P_f = 0$; σ_o = normalizing strength for a unit volume of material loaded in tension; V = specimen volume, and m = measure of the spread in strength values and is called the Weibull modulus. The higher the m value, the tighter the strength distribution, ie, the lower the variability. For conservative design, σ_μ is set to zero, reducing the Weibull distribution to a two parameter description.

Under conditions other than tensile loading, the stress distribution in a body is nonuniform. To account for this, a loading factor k is used to calculate the effective volume under stress and kV replaces V. This analysis assumes that flaws are randomly distributed throughout the volume. In many ceramics, glass in particular, nearly all failures occur from surface flaws. If that is the case the volume term is replaced with an area term.

To obtain the Weibull parameters, the strengths of $N > 30$ samples are measured and ranked from lowest to highest. The failure probability is then calculated using an estimator:

$$P_f = \frac{n}{N+1} \tag{9}$$

where $N =$ number of specimens and $n =$ rank of sample. The data are plotted as ln ln$[1/(1-P_f)]$ versus ln σ according to equation 10, which is derived from equation 8.

$$\ln \ln\left(\frac{1}{1-P_f}\right) = \ln V - m \ln \sigma_o + m \ln \sigma \tag{10}$$

The terms V (or kV) and σ_o are usually grouped together as a single term σ_o' called the characteristic strength, which is specific to the test specimen geometry and volume. The parameters m and σ_o' can be obtained from the slope and intercept, respectively. Typical m values for ceramics range between 5 and 20 (18); 5 indicates a high variability in the strength and 20 a relatively low strength variability. Detailed information on the standard procedure for determining and reporting Weibull parameters is available (19).

Compressive Strength. Ceramics are much stronger in compression than in tension and are frequently used in applications where they bear compressive loads. Under excessive compressive loads ceramics fail in a brittle manner just as they do in tension; however, the measured compressive stresses are typically eight times greater than the measured tensile stresses for the same material (12). In compression, the failure process can begin with microplastic deformation, not the growth of preexisting flaws. Measured compressive strengths are shown in Table 2. Although there is limited data relating microstructure to compressive strength, compressive strength often shows an inverse relationship to the square root of the grain size. Porosity effects on compressive strength have been modeled using the same type of relation used for Young's modulus (eq. 2).

2.3. Fracture Toughness. The fracture criterion was defined by a critical value of the crack tip stress intensity, known as the fracture toughness, K_C. Ceramics often fail in pure tension, designated the mode I stress intensity, and K_{IC} replaces K_C in equation 6. Thus σ_{fracture}, the applied tensile stress at which fracture occurs, is a function of the flaw size and K_{IC}. A crack propagates catastrophically when the stress intensity factor at the crack tip reaches the critical value required for bond breakage, and when its rate of change with respect to the crack length is positive. Thus the critical stress intensity, K_{IC}, required for bond rupture is considered to be a material constant.

Under some circumstances the crack tip stress intensity factor is different than what the far-field stresses would indicate because of microstructural effects

behind the crack tip. These include effects due to the presence of crack bridging fibers, whiskers, and grains. Often far-field values indicate the crack is propagating at a stress intensity value higher than K_{IC}, and this apparent value usually increases as crack length increases. Despite indications to the contrary, bonds continue to break at the same value of the stress intensity; however, the crack tip is being shielded from some of the applied stress intensity. To minimize confusion about K_{IC}, it has been suggested that the far-field value of the stress intensity be called K_{applied}. When there are no microstructural features that effectively reduce the crack tip stress intensity, such as in glasses, the crack tip stress intensity is accurately represented by the far-field values, and K_{applied} equals K_{IC}. In this case, equation 6 can be used to predict what size flaw a material can tolerate at a given stress level.

K_{IC} measurements can be made by introducing a crack of a known size and a specific geometry in a body and then loading the body until catastrophic failure occurs. The shape factor Y, used to account for different flaw and loading geometries, can be found in reference handbooks (8). An alternative approach for determining K_{IC} consists of measuring the length of surface cracks introduced using a sharp indenter (20). The low fracture toughness, in units of $\text{MPa} \cdot \text{m}^{1/2}$, of ceramics is demonstrated by values of 0.75 for glass, 2.7–4.2 for alumina, 7–10 for Si_3N_4, and 8–9 for partially stabilized ZrO_2, as compared to 11–13 for common woods perpendicular to grains, 6–20 for cast iron, 46 for tool steel, 120–153 for high strength steel, and 100–350 for pure ductile metals, eg, Cu, Ni, and Ag (21).

R-Curve Behavior. Ceramic toughening efforts have focused on the property of some ceramics to exhibit increased apparent fracture toughness as cracks grow. This increase is seen in terms of the far-field value of the stress intensity required to propagate the crack. An important consequence of this effect, which is commonly referred to as R- or T-curve behavior, is that the material has increased damage tolerance because there is a crack size regime in which the strength is independent of the crack size. The underlying basis of R-curve behavior is that the crack tip stress is redistributed, either to immediately adjoining material, as in the case of the process zone formed in transformation toughened materials, or to regions far removed from the crack tip, as in the case of fiber-reinforced ceramics. One reason for the interest in crack bridging mechanisms is that these toughening mechanisms should operate over a broad range of temperatures. Characteristics of R-curve mechanisms are that they are activated only as the crack advances, the number of activated shielding elements increases as the crack grows, and the measured fracture toughness saturates when the generation rate of shielding elements equals the rate at which elements become inactive.

One implication of R-curve behavior is that the measured fracture toughness is not a material constant equal to K_{IC}; rather it is a function of the crack length. The material can still be considered to have a constant toughness. However, there are microstructural influences that affect the effective stress intensity K at the crack tip. R-curves depend on crack size, loading conditions, and component geometry (22). Microstructural effects influencing R-curve behavior include grain size, shape, and orientation, grain boundary toughness, and thermal expansion anisotropy. In alumina, where R-curve behavior occurs because of ligamentary bridges formed by grains behind the crack tip, grain size determines

the scale of grain pullout (23). At small grain sizes the bridging effect appears to be insignificant.

Transformation Toughening. Transformation toughened materials exhibit enhanced toughness because of a process zone at the crack tip that consumes energy that would otherwise be used in the creation of fracture surface. Various processes at the crack tip have been postulated to consume energy such as the phase transformation from tetragonal to monoclinic zirconia, microcracking, and deviation of the primary crack around the transformed particles. The zone can also be thought of as a region that partially shields the crack tip from the far-field stresses. Significant toughening cannot occur until the process zone has grown sufficiently to extend behind an advancing crack tip as shown in Figure 2. A comprehensive review of transformation toughening of ceramics is provided (24).

The transformation toughening mechanism has been most successfully exploited in ZrO_2-based materials, where the phase transformation of interest is from tetragonal to monoclinic ZrO_2. Microcracking may also play a role in the transformation toughening of ZrO_2 materials because of the extra energy required to produce additional fracture surface. Toughness enhancements of almost 100% (from 5.2 to 9.5 $MPa \cdot m^{1/2}$) have been achieved in ceramics such as Al_2O_3 by adding ZrO_2 as a second phase (24).

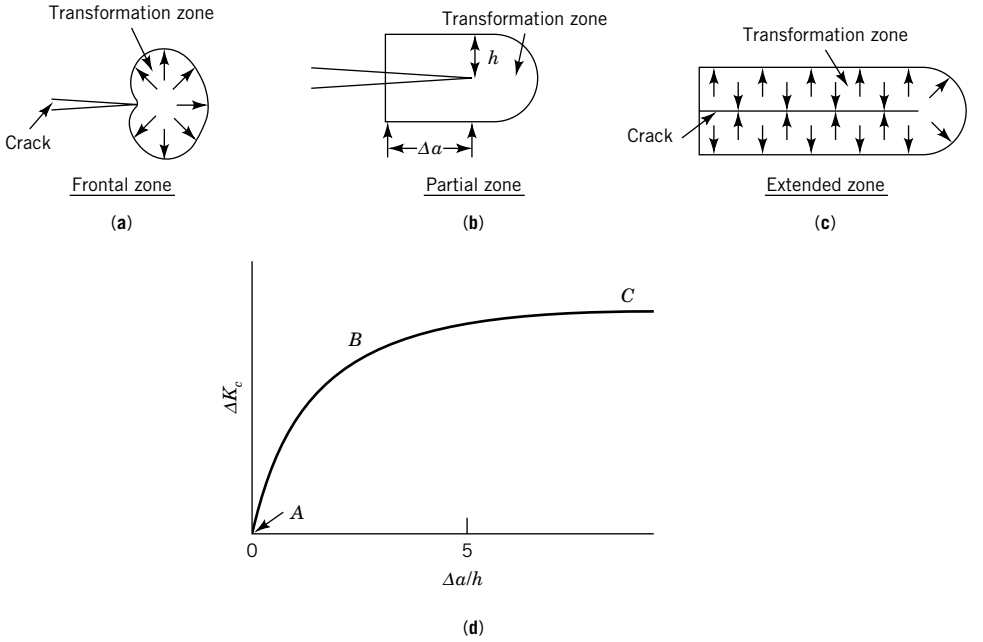

Fig. 2. A schematic of a zirconia body containing a propagating crack: (**a**) the frontal zone of the transformed material; (**b**) the partial zone defining Δa and h; (**c**) the extended and the transformation and extended zones; and (**d**) change in fracture toughness as a function of growth of the transformation zone, where A represents the frontal zone; B, the partial zone; and C, the extended zone.

Oxides such as CaO, MgO, and Y_2O_3 are added to ZrO_2 to stabilize the tetragonal phase at temperatures below the tetragonal to monoclinic phase-transition temperature. Without stabilizer, the phase transition occurs spontaneously at temperatures below 850–1000°C, and no fracture toughness enhancement can occur (25).

Toughening Mechanisms in Composite Ceramics. Significant toughening has been achieved by fabricating whisker- and fiber-reinforced ceramic composites, and metal–ceramic composites (see COMPOSITE MATERIALS, SURVEY). Toughening primarily results from crack bridging and/or crack deflection, both of which reduce the crack tip stress intensity. Crack deflection, which occurs when the reinforcement debonds from the matrix, changes the orientation of the crack relative to the stress application direction, changing the stress distribution around the crack such that the stress intensity at the crack tip is reduced. When a reinforcement phase bridges the crack behind the crack tip, it supports some of the applied load, and therefore shields the crack tip from some of the applied stress intensity. Crack tip shielding results in R-curve behavior and the ability of these materials to resist catastrophic failure as shown in Figure 3.

Crack deflection toughening resulting from debonding along interfaces between the matrix and reinforcement phase has been covered extensively in the literature (26–28). Crack bridging, which plays the largest role in enhancing the toughness, depends on intact whiskers or fibers being able to pull out of the matrix behind the crack tip. A very large amount of energy can be consumed in this process that would otherwise be used to propagate the crack. The stress–strain behavior of a fiber-reinforced composite in Figure 3 shows that during the initial stages of loading, the composite exhibits the same behavior as an unreinforced matrix, ie, it is linear elastic. At point A the matrix begins to crack and the slope of the stress–strain curve begins to decrease. At point B

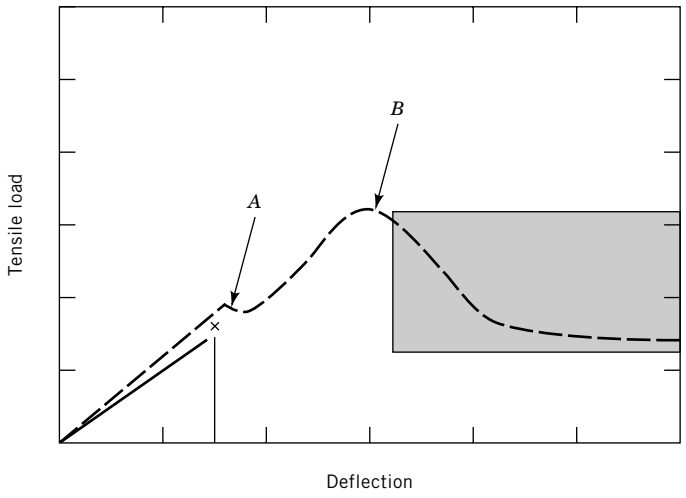

Fig. 3. Tensile stress–strain curve for (——) unreinforced ceramic and (- - - -) fiber-reinforced ceramic composite. A represents the point where the matrix begins to crack; B, where the reinforcement begins to fail and the section where reinforcement pulls out of the matrix. X indicates the point of catastrophic failure.

the fibers begin to fail and the load the body can support diminishes. The area under the stress–strain curve, past the point where the matrix begins to crack, represents the energy absorbed during fiber debonding and pull-out. Many composites exhibit very large strains to failure and retain some load-bearing capability even after the integrity of the matrix has been lost.

Whiskers or fibers must be able to debond and pull out of the matrix in order for significant toughening to occur. Thus the parameters controlling the toughness of a composite are the interfacial strength and the interfacial frictional or pullout stress, τ, which has to be overcome before the reinforcement slides out of the matrix. If the interfacial strength is too high, the fibers break instead of debonding, and the value of the frictional stress is irrelevant. Methods for controlling the interfacial strength include choosing reinforcement and matrix materials that do not react, and coating the fiber with nonreactive or low strength porous coatings (29). Low τ values produce the greatest toughening with respect to fiber pullout.

Composites have also been made where strengthening is the goal. A high pullout stress, τ, is one of the important parameters for higher strength because high values allow load transfer from the matrix to the high strength fibers. The opposing effects of the pullout stress, τ, on the toughness and strength, highlight the importance of the design of the reinforcement-matrix interface in the overall design of composites. The role of the interface is covered (30).

Metal–ceramic composites, including those made by *in situ* oxidation of infiltrated molten metal (31), have high toughness values that result from residual ductile metal that bridges the crack behind the crack tip (32). Because of the large amount of plastic work required to cause these elements to fail, there is an increase in the amount of energy, or applied stress intensity, required to propagate a crack through the composite. Composites of this type exhibit fracture toughness values as great as three times the matrix toughness (33).

Ferroelasticity. Ferroelastic materials contain domains that can be switched by an applied stress (34) in a manner analogous to magnetic domain switching in ferromagnetic materials. A hysteresis loop between the applied field or stress and the induced state, and a permanent induced state when the applied field is removed, are characteristic of domain switching for both of these properties. The permanent state of a ferroelastic is the permanent strain induced by the applied stress. Many ceramics that exhibit ferroelasticity also exhibit ferromagnetism and/or ferroelectricity, such as $BaTiO_3$ and lead zirconate titanate (PZT). Toughening occurs because energy is absorbed in the switching of the domains.

Tetragonal zirconia is a structural ceramic that exhibits ferroelasticity and the toughness enhancement has been estimated to be as high as 5 $MPa \cdot m^{1/2}$. An example of a partial hysteresis loop for this material is shown in Figure 4 (35). Domains do not have to be present prior to the stress application because stresses can also nucleate domains (36). Domain nucleation and additional fracture surface generated by fracture along domain boundaries appear to contribute to the toughening.

2.4. Plasticity. Although even at elevated temperatures [$>0.6\ T_m$ (melting temperature)] mechanical failure of ceramics is dominated by brittle fracture, plastic deformation mechanisms often precede brittle fracture. Plastic

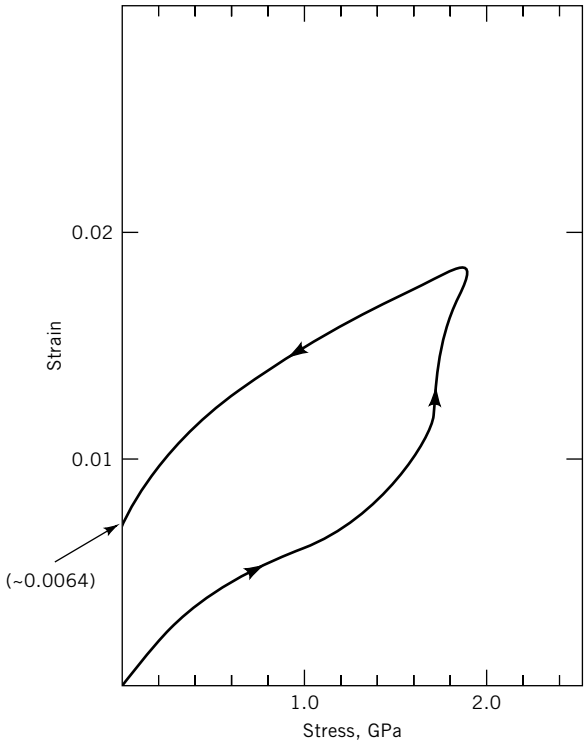

Fig. 4. Partial hysteresis loop for a ferroelastic material. After the applied stress is removed a permanent strain $\varepsilon \sim 0.0064$ remains (see eq. 1).

deformation is also important because of the role it plays in net shape forming operations such as extrusion, which require extremely high strain rates in a deformation regime known as superplasticity (37). In the lower range of the elevated temperature mentioned above, plastic deformation of crystalline ceramics can occur by slip. In a slightly higher temperature range ($>0.7\ T_m$), plastic deformation can also occur by grain boundary sliding and softening of secondary phases such as glass.

Plastic deformation by slip involves one atom plane sliding past another, or twinning by homogeneous shearing. Once slip occurs there is permanent deformation of the material. As the stresses at which slip is observed are significantly lower than those required to slide perfect planes of atoms past each other, defects that allow this motion to occur must be present. The primary mechanism of slip at relatively low stresses in polycrystalline materials is the motion or glide of line defects called dislocations. Dislocation motion allows bonds to break at relatively low applied stresses because dislocation motion occurs by sequential bond breakage. This is somewhat analogous to fracture. The primary difference between dislocation motion and fracture is that bonds immediately reform after a dislocation has passed, whereas they remain ruptured after a crack front passes.

Slip usually occurs on the planes that have the highest atom density and are the greatest distance from adjacent planes. Therefore the slip systems that

can be activated in a crystal depend primarily on crystal structure, and those crystals with the highest symmetry, eg, cubic, have the most available slip systems. Slip systems and the temperatures at which they are activated are available (18).

If a ceramic single crystal is suitably oriented with respect to the applied stress direction, deformation can occur through dislocation motion. The rate of plastic deformation depends on the number of dislocations and their velocity. Although suitably oriented ceramic single crystals such as MgO deform plastically at low temperatures by slip, polycrystalline forms of the same material act in a brittle manner because of geometrical constraints. Plastic deformation in ceramics by slip is also suppressed by the large amount of energy required to move dislocations, especially for covalently bonded ceramics such as SiC and Si_3N_4. As temperature increases, plastic deformation by slip becomes easier because of the increased amount of energy available for dislocation glide. Other plasticity mechanisms also become activated at elevated temperature but despite the increased plasticity at these temperatures, failure ultimately occurs in a brittle manner when cracks nucleate at grain boundaries. The total strain prior to fracture in a tensile test conducted at elevated temperature is usually $<1\%$.

The processes leading up to failure at elevated temperatures are known as creep. Figure 5 shows a typical creep curve divided into four regions. The first region, often ignored, represents the instantaneous deformation that occurs when a load is applied. The second region usually shows decreasing creep rate and is known as primary or transient creep. The third region, known as steady-state or secondary creep, is the most important for lifetime predictions. In tensile creep tests fracture often occurs in this region. The fourth region is known as tertiary creep and in this region the deformation rate accelerates just prior to complete failure. Fracture occurs as various types of creep damage accumulate. Damage includes loss of load bearing area from the formation of pores or cavities,

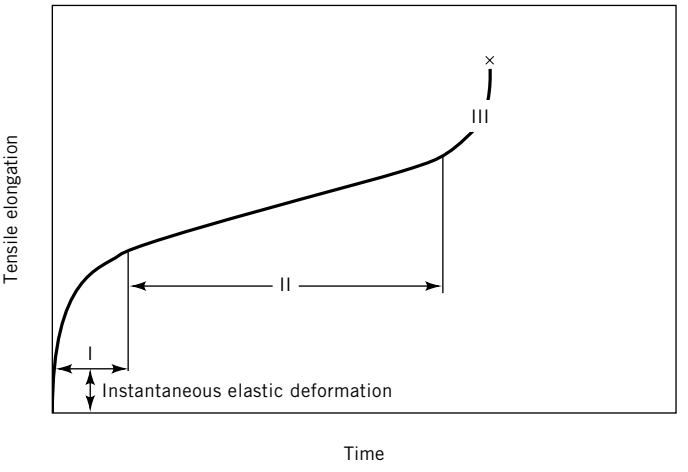

Fig. 5. Tensile elongation vs time demonstrating creep behavior of ceramics. Section I is primary creep; II, secondary or steady-state creep; III, tertiary creep; and X, fracture.

linking of the cavities to form cracks, and environmental degradation of the microstructure. Increased temperature or stress increases the creep rate and reduces the time to failure.

Polycrystalline ceramics exhibit diffusional creep, in which deformation occurs by diffusional flow of atoms to and from grain boundaries, either by diffusion through the lattice (Nabarro-Herring creep), or along the grain boundaries (Coble creep) (38,39). At temperatures close to the melting point, creep may also occur by dislocation motion, and this process is termed lattice creep . Creep can also occur by grain boundary sliding in materials with and without liquid grain boundary phases. Diffusional creep and creep by grain boundary sliding are categorized as boundary creep mechanisms. Detailed information on creep mechanisms can be found in the literature (38,40).

In the steady-state creep regime of ceramics, almost all creep mechanisms fit a strain rate dependence of the form (18):

$$\dot{\varepsilon} = \frac{A^* DGb}{kT}\left(\frac{b}{l_g}\right)^{m^*}\left(\frac{\sigma}{G}\right)^{n^*} \tag{11}$$

where $\dot{\varepsilon}$ = strain rate; A^* = dimensionless constant; D = diffusion coefficient (exponential temperature dependence); G = shear modulus; b = Burgers vector; k = Boltzmann's constant; T = temperature; l_g = grain size; σ = applied stress; n^* = stress exponent, which commonly has values of 1–5; and m^* = grain size exponent, which commonly has values of 0–3. Analysis of creep data using equation 11 usually allows a specific creep mechanism to be identified, based on the stress and grain size exponents. Once the creep mechanism has been identified the deformation kinetics can be determined and lifetime predictions can be made. Creep in some ceramics is sufficiently well understood over a broad range of conditions that the deformation behavior and theoretically predicted behavior can be displayed on maps known as Ashby plots (41).

Equation 11 shows that a larger grain size favors increased creep resistance. The potential detrimental effects of second phases are an important consideration for ceramics that require dopants as sintering aids. Impurities affect the diffusion coefficient and may end up as grain boundary phases, which are often glassy in nature.

Plastic deformation is commonly measured by measuring the strain as a function of time at a constant load and temperature. Deformation strain can be measured under many possible loading configurations. Because of problems associated with the preparation and gripping of tensile specimens, plastic deformation data are often collected using bend and compression tests.

2.5. Hardness. Although large-scale deformation in ceramics usually occurs only at elevated temperature, localized, constrained compressive loading can produce plastic deformation even at room temperature. Hardness (H) is a measure of the resistance of a material to deformation, in particular the resistance to plastic deformation during surface penetration. Hardness is related to the bond strength. Because covalent and multivalent ionic bonds are strong and highly directional in nature, slip is very difficult in these cases, and ceramics containing these bonds are generally the hardest materials (42). The ratio of the distance, a, between planes of atoms and the spacing, b, of the atoms in the plane

also plays an important role in how easily planes of atoms slide past each other. Materials with small a/b ratios tend to possess a high resistance to slip, and are consequently harder (5). In contrast, glasses, which have strong covalent bonds and do not have any dislocation activity, are softer than crystalline ceramics. This is partially due to their low bond densities compared to polycrystalline ceramics. In some glasses, a significant portion of the deformation under compressive loading results from irreversible compaction of the glass, rather than from plastic flow.

Hardness is determined by measuring the penetration (depth or area) when a harder material, such as diamond, is pushed into the surface of the material of interest under a specified load. True hardness is defined as the force divided by the projected area. Vickers hardness tests, which employ a pyramid-shaped indenter, are frequently used to characterize ceramics; however, Vickers hardness calculations normally employ total surface area rather than projected area (43). Measurements are made on the diamond impression shown in Figure 6. Vickers hardness, H_v, is calculated using

$$H_{V,\,\text{totalarea}} = \frac{0.46\,P}{a^2} \tag{12}$$

where P = indentation load and a = half-length of Vickers impression diagonal. Hardness is normally expressed in units of GPa but Vickers hardness numbers are also expressed in units of kg/mm^2. Many other hardness scales are used; however, conversions between scales are not always possible (43). Hardness values of some ceramics are compared to common metals in the following table.

Material	Hardness, GPa
lead	0.07
copper	0.86
steel	2.23
cast iron	1–7
glass	6–7
zirconia (partially stabilized)	10–11
silicon nitride	8–19
alumina	18–23
silicon carbide	20–30
diamond	98

Hardness decreases with increasing porosity. Ceramics deform plastically more readily at higher temperatures and therefore hardness decreases with increasing temperature according to

$$H = H_o\left(1 - \frac{T}{T_o}\right) \tag{13}$$

where H_0 = hardness at 0 K and T_0 = temperature in Kelvin at which hardness goes to zero (44). Further information on hardness of ceramics is available (45,46).

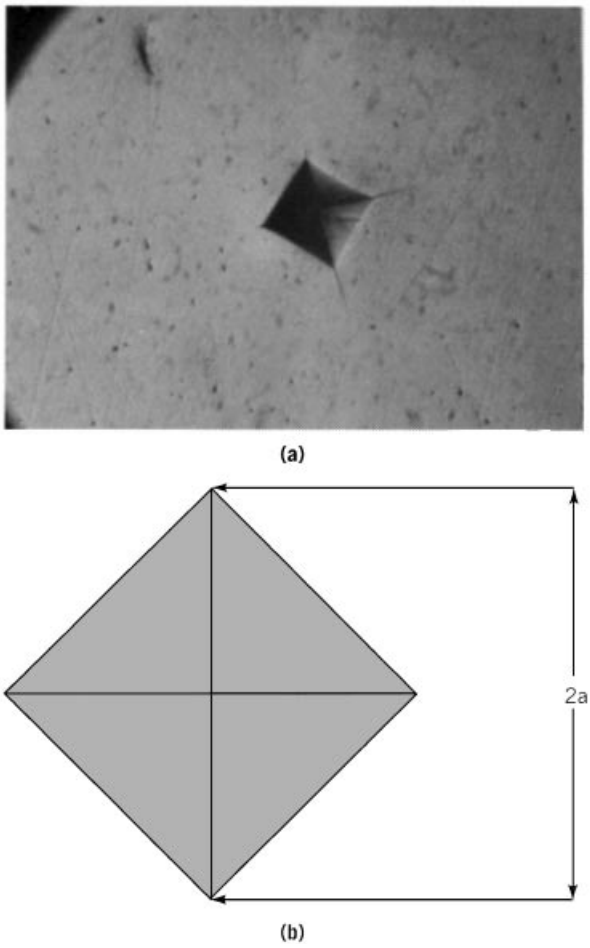

Fig. 6. (**a**) Vickers indentation in zirconia at 200 X. (**b**) Schematic of a Vickers indentation showing the dimension used in Vickers hardness determinations.

2.6. Subcritical Crack Growth. At low and modest temperatures, under certain environmental conditions, the strength of many ceramics, especially glasses, can degrade with time under mechanical loading. This phenomenon, referred to as static fatigue or delayed failure, is the result of subcritical crack growth (SCG). A preexisting crack grows slowly at an applied stress intensity lower than that necessary, ie, the critical value K_{IC}, to propagate a crack without environmental influences. SCG is pernicious because a flaw grows slowly at stresses far below the expected failure load until the flaw is large enough to satisfy the Griffith criterion, at which point failure occurs catastrophically.

The mechanism of subcritical crack growth is the reaction of the corrosive medium with highly stressed bonds at the crack tip. As such the mechanism is often referred to as stress corrosion cracking. In silica, in the absence of stressed bonds, the rate of the reaction between the bonds and corrosive media such as water is very low. The introduction of strain energy into crack tip bonds

increases the activity of the bond. For silica glass in water, attack and bond breakage occurs by the following reaction (47):

$$\underset{\text{(water)}}{\text{H—O—H}} + \underset{\text{(ionic/covalent bond in glass)}}{\text{—Si—O—Si—}} \longrightarrow \underset{\text{(2 silanol groups)}}{\text{—Si—OH}} + \text{HO—Si—}$$

in which weak bonds between silanol groups replace strong silicon–oxygen bonds. Similar reactions occur with ammonia, methanol, and other liquids (48).

The plot of crack velocity v, as a function of applied K_I, is usually divided into three regions as shown in Figure 7. In region I, v exhibits a power law dependence on K_I. The stress intensity determines the bond reactivity and therefore the kinetics of the chemical reaction at the crack tip and the rate of bond breakage. An increase in the reactive species concentration, eg, water, and increased temperature shift region I to lower K_I. Region II is determined by the rate at which the corrosive chemical species travels to the crack tip, and is insensitive to K_I. The Region II plateau velocity depends on the environment. For example, increasing relative humidity raises the plateau. In Region III, v is a strong function of K_I and believed to be independent of environment. Crack velocity in regions I and III can be approximated by an empirical relationship of the form

$$v = AK_I^n \tag{14}$$

where A = material constant and n = subcritical crack growth susceptibility constant. The relationship in equation 14 is most useful for region I because this

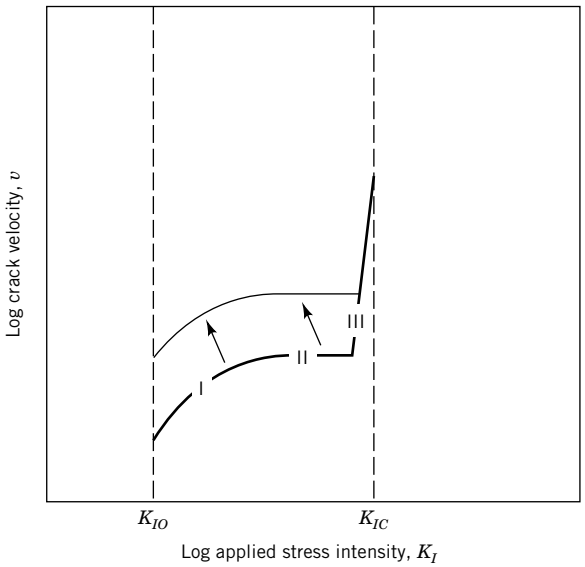

Fig. 7. Crack velocity, v, as a function of the applied stress intensity, K_I. Water and other corrosive species reduce the K_I required to propagate a crack at a given velocity. Increasing concentrations of reactant species shift the curve upward. Regions I, II, and III are discussed in text.

represents the majority of a ceramic component's lifetime. At K_{IC}, bonds break without environmental assistance and the crack becomes critical. There is also a threshold K_I, known as the stress corrosion limit or the fatigue limit, K_{IO}, below which crack growth ceases; however, K_{IO} is usually a practical limit dictated by how low a velocity can be measured, for example, 1×10^{-11}m/s. Information of the type presented in Figure 7 can be used to determine what applied K_I should be used to ensure that no crack propagation occurs, or to predict component lifetime. Materials with low n values are most susceptible to SCG. Values of n range from 15 for soda lime silica glass to 35 for silica glass, and from 90–100 for oxides such as MgO-stabilized ZrO_2.

2.7. Impact and Erosion. Impact involves the rapid application of a load to a relatively small area. Two types of stress can arise during the impact; a localized stress at or near the impact point, and/or a macroscopic stress. Much of the kinetic energy from the impacting object may be transformed into strain energy for crack propagation. If the impact is from a blunt indenter, a crack called a Hertzian conoid usually forms from excessive tensile stresses around the point of contact. If, after the Hertzian conoid is formed, the impacting object still possesses a significant amount of kinetic energy, further damage may occur in the form of radial cracks and circumferential cracks. Sharp indenter impact can also produce Hertzian cone cracks as shown in Figure 8. If the impact load is relatively large and sustained, a macroscopic stress may be imposed on the target body causing it to bend. This may lead to excessive tensile stresses on the opposite face of the body, crack initiation, and catastrophic failure. Failure can also occur if erosion reduces the cross section and load-bearing capacity of the component, causes a loss of dimensional tolerance, or causes the loss of a protective coating. Detailed information on impact and erosion is available (49).

External factors affecting a ceramic's response to impact include the velocity, size, and shape of the impacting object, and its angle of incidence. Impacting particles do not have to be hard or tough materials to cause damage and erosion. For instance, water at high velocities, eg, rain on aircraft windshields, can have an extremely erosive effect because of the high localized stresses that it produces. Another mechanism of failure for liquid impact is the generation of shock waves that interact with preexisting flaws producing crack growth. Material and microstructural characteristics that influence a ceramic's impact resistance include density, elastic modulus, crystalline anisotropy, hardness, fracture toughness, strength, grain size, defects such as pores, and the presence of second phases. There are limited data quantifying the relationship between impact strength and microstructural parameters.

Impact resistance is determined using flyer plate impact tests, long rod impact tests, Hopkinson bar tests (50) , and the liquid jet technique (51). Impact damage resistance is often quantified by measuring the post-impact strength of the ceramic.

2.8. Tribiological Behavior. Tribological performance of ceramics, which includes friction, adhesion, wear, and lubricated behavior of two solid materials in contact, has been reviewed (52). This topic is receiving increasing attention because of applications of ceramics such as bearings, gears, and seals, and because of ceramic coatings being evaluated for micro-electromechanical systems (MEMS).

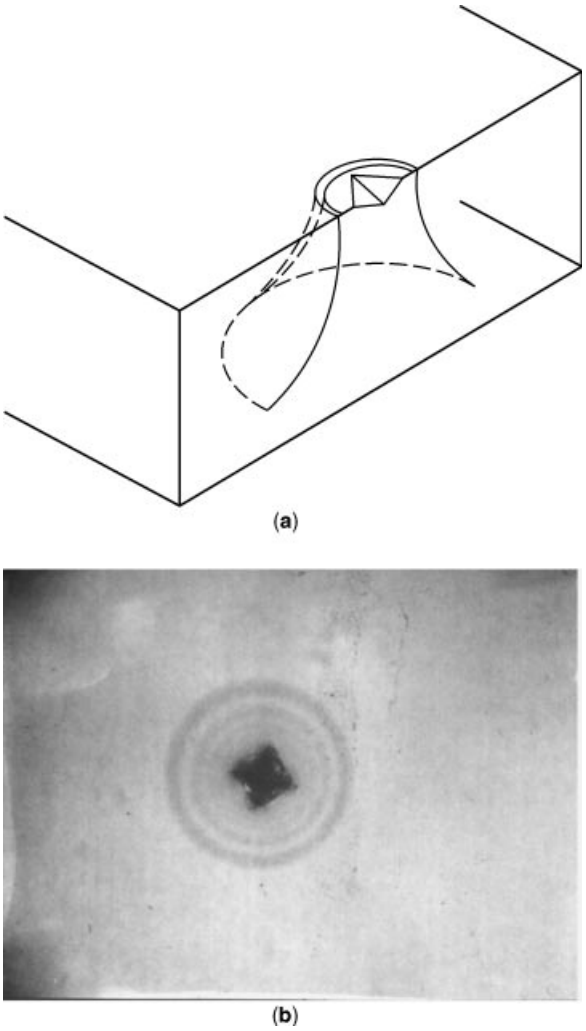

Fig. 8. (**a**) Schematic of a Vickers indentation-induced Hertzian cone crack. (**b**) View from the bottom of an aluminosilicate glass block of a Vickers indentation-induced Hertzian cone crack.

Friction and Adhesion. The coefficient of friction μ is the constant of proportionality between the normal force P between two materials in contact and the perpendicular force F required to move one of the materials relative to the other. Macroscopic friction occurs from the contact of asperities on opposing surfaces as they slide past each other. On the atomic level friction occurs from the formation of bonds between adjacent atoms as they slide past one another. Friction coefficients are usually measured using a sliding pin on a disk arrangement. Friction coefficients for ceramic fibers in a matrix have been measured using fiber pushout tests (53). For various material combinations (21):

Materials	μ
clean metals in air	0.8–2
steel on ceramics	0.1–0.5
ceramic on ceramic	0.05–0.5
high temperature lubricants (MoS_2, graphite)	0.05–0.2

Factors that affect μ include loading geometry, microstructure, crystal orientation, surface chemistry, environment, temperature, and the presence of lubricants.

Wear. Ceramics generally exhibit excellent wear properties. Wear occurs by two mechanisms: adhesive wear and abrasive wear (21). Adhesive wear occurs when interfacial adhesion produces a localized K_I when the body on one side of the interface is moved relative to the other. If the strength of either of the materials is lower than the interfacial shear strength, fracture occurs. Lubricants (see LUBRICANTS AND LUBRICATION) minimize adhesion between adjacent surfaces by providing an interlayer that shears easily. Abrasive wear occurs when one material is softer than the other. Particles originating in the harder material are introduced into the interface between the two materials and plow into and remove material from the softer material (52). Hard particles from extrinsic sources can also cause abrasive wear, and wear may occur in both of the materials depending on the hardness of the particle.

Generally the harder the ceramic, the better its wear resistance; however, other properties such as fracture toughness may play the dominant role. If a ceramic is mated with a metal hardness is the determining factor, but when a ceramic is mated with another ceramic fracture toughness appears to determine the wear rate (54).

2.9. Thermal Stresses and Thermal Shock. Thermal stresses arise when a body is heated or cooled and constrained from expanding or contracting. Thermal stresses can lead to fracture and catastrophic failure when the magnitude of the thermal stress exceeds the strength of the ceramic. Factors that contribute to the generation of large thermal stresses and the failure of ceramics under these stresses are low thermal conductivities, which produce large temperature gradients, and the lack of a stress relief mechanism such as plastic deformation. Approaches used to minimize thermal stresses include matching the expansion of ceramics with the expansions of the materials to which they are joined (55), minimizing temperature gradients, minimizing cross-sectional thickness changes to ensure that the body heats or cools uniformly, keeping the body at its operating temperature, and heating and cooling slowly.

Residual thermal stresses can occur in ceramics, especially in glasses, when they are cooled from elevated temperatures, and faster cooling of one region freezes in a structure that subsequently is unable to contract as much as another. This produces a situation wherein the regions that initially cooled more quickly are under compression and the slower cooling regions are under tension. Because tensile stresses are normally undesirable, annealing procedures are used to eliminate the residual stresses. Beneficial residual compressive

surface stresses, which effectively strengthen the glass, are produced by a rapid cooling procedure known as thermal tempering.

When heating or cooling is extremely rapid, such as when a body is removed from a furnace and immersed in ice water, large thermal gradients produce very high, transient stresses. Rapid temperature changes, known as thermal shock, can lead to immediate failure of the body, or a degradation in the strength of the body resulting from the generation and propagation of cracks, or the growth of preexisting flaws. Thermal shock resistance (TSR) is the resistance to thermal shock-induced strength changes. TSR is usually quantified in terms of the temperature change, ΔT, below which no strength degradation occurs.

TSR depends on the conditions of thermal shock, the material, and the intended application of the material. TSR parameters are broadly divided into two groups, those based on conditions under which crack nucleation is favored, and those under which crack propagation is favored. For the former situation high TSRs are found for materials with low E and α, and high σ and thermal conductivity. For conditions favoring crack propagation, high TSRs are found for materials with high E and fracture surface energy, γ, and low σ. A compendium of TSRs is available (56). An example of a commonly used TSR parameter is

$$\Delta T = \frac{\sigma\,(1-\nu)}{\alpha E} \tag{15}$$

where $\sigma =$ strength, $\nu =$ Poisson's ratio, $\alpha =$ coefficient of thermal expansion, and $E =$ Young's modulus. TSR values, calculated using equation 15 and typical values of σ, ν, α, and E are shown in Table 3.

TSR is commonly measured by heating ceramics to various temperatures and then quenching them in a liquid medium. The critical temperature difference ΔT_{crit}, which causes severe damage, is used as a measure of the TSR. A common approach for quantifying the damage from thermal shock is to compare the strength of quenched and unquenched specimens. Another test utilizes thin circular disks heated rapidly with tungsten halogen lamps (57).

2.10. Cyclic Fatigue. Cyclic fatigue is the weakening and subsequent failure of a material during cyclic loading, often at stress levels significantly lower than those required to cause failure under static loading. Cyclic stresses

Table 3. **Thermal Shock Resistance Parameters**

Material	Strength, MPa[a]	Poisson's ratio	Coefficient of thermal expansion, $\times 10,^{-6}\,^{\circ}C^{-1}$	E, GPa[a]	TSR parameter, °C
alumina	345	0.22	7.4	380	96
pyrex	70	0.20	4.6	70	170
silicon carbide	414	0.17	3.8	400	230
Y-TZP[b]	745	0.23	10.5	220	248
silicon nitride	310	0.24	2.4	172	650
LAS[c]	138	0.27	−0.3	70	4860

[a] To convert MPa to psi, multiply by 145.
[b] Y – TZP = yttria – stabilized tetragonal zirconia polycrystal.
[c] LAS = lithium aluminosilicate.

can be produced by repeated heating and cooling, by vibrations, and in applications in which the component is repeatedly loaded and unloaded. Ceramics were not recognized to exhibit cyclic fatigue (58) until the late 1980s when it was shown that cyclic fatigue occurs in ceramics under compressive loading (59). In ceramics that show crack bridging, cyclic fatigue is largely a result of the loss or destruction of ligamentary bridges when the crack closes. Some of the difficulties in identifying cyclic fatigue mechanisms in ceramics are related to the difficulties in obtaining reliable data using conventional cyclic fatigue testing, in which the failure stress is determined vs. the number of cycles to failure. An alternative approach for ceramic cyclic fatigue testing is based on the repeated indentation of a polished surface until chipping occurs (60).

3. Fracture Analysis

Fracture analysis, also known as fractography, plays an important role in understanding the relationships between the microstructure and mechanical properties, and the conditions that lead to failure (see FRACTURE MECHANICS). Systematic examination and interpretation of fracture markings and the crack path can often be used to reconstruct the sequence of events and stresses that led to failure. Fractography also plays an important role in the design and development of ceramic components because it helps differentiate whether failure occurred because the material was weakened by the introduction of processing and handling flaws, or because the applied stress exceeded the design stress.

Well-established fractographic techniques are available for determining crack propagation direction, failure origin location, estimating the failure stress, identifying what types of flaws are present, and for identifying local events that initiated failure (42,61,62). A significant amount of information about crack growth and failure can be determined using the fracture surface markings and the crack path. Some of the most useful fracture markings include crack branching patterns; twist hackle; Wallner lines; and arrest lines. At crack velocities approaching the terminal velocity, the fracture mirror, mist, and hackle, so called because these three terms aptly describe their appearance, are generated and can be seen on the fracture surface. These features are readily apparent for glasses as seen on the fracture surface in Figure 9. Fracture surface markings are influenced by, and therefore can provide information about the stress magnitude and orientation, crack velocity, interactions of the crack with microstructural inhomogeneities and stress pulses, flaw size and shape, and the test environment. The crack path provides information about the stress state at different positions in the body. The crack pattern can be a good indication of the conditions that gave rise to a certain stress state, such as thermal shock, impact, and twisting.

Fracture markings can be used to locate the failure origin, which is the discontinuity or flaw that caused the applied stress to be amplified locally. Once the failure origin has been located, the failure stress can be estimated using the flaw size and equation 6, or the distances to the boundaries of the mirror, mist, and hackle (whichever is most evident) and the following relation (63)

$$\sigma_{\text{fracture}}\sqrt{r_i} = A_i \tag{16}$$

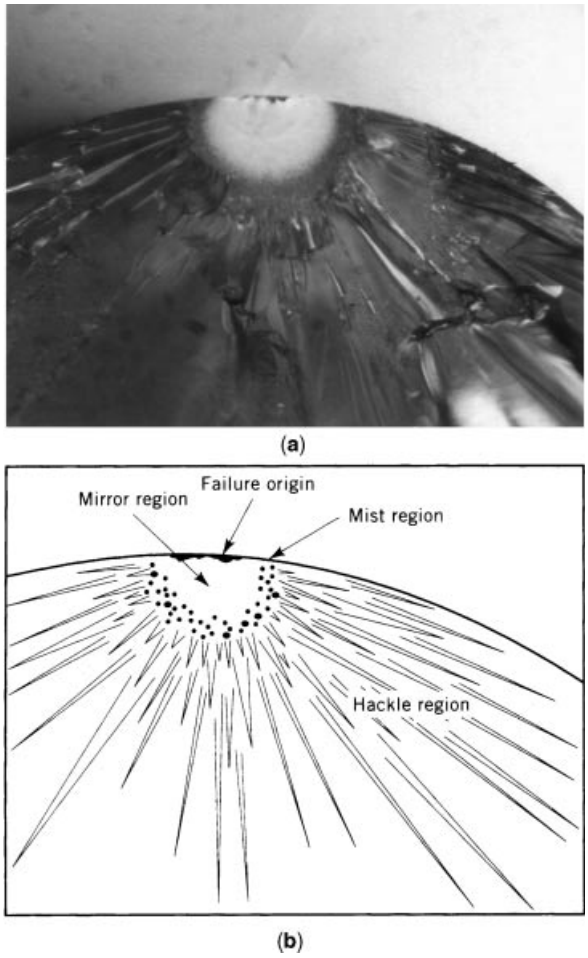

Fig. 9. (**a**) Optical micrograph of the fracture surface of a glass rod at 38 X. (**b**) Characteristic fracture markings such as mirror, mist, and hackle and the failure origin are indicated on the fracture surface schematic.

where $r =$ radius; $A =$ constant [values for various ceramics can be found in the literature (63)] and; $i = 1$, 2, or 3 refers to the mirror-mist, mist-hackle, and hackle-branching boundaries. If the ceramic body is small and the failure stress is extremely low, the mirror may extend over the entire fracture surface, and mist and hackle are absent.

A standard is available that describes an efficient and consistent methodology for conducting fractography (64). Simple instruments such as a pocket magnifying eyepiece or an optical microscope are often sufficient for obtaining critical information. As with any detective work, it is important to maintain careful records and to pay close attention to details in the reconstructions of the conditions under which fabrication and failure occurred. Seemingly unimportant details of fabrication, service, and/or the conditions under which failure occurred can frequently be the key to determining the cause of failure.

BIBLIOGRAPHY

"Properties and Applications of Ceramic Materials" under "Ceramics" in *ECT* 2nd ed., Vol. 4, pp. 793–832, by H. Palmour III, North Carolina State of The University of North Carolina, in *ECT* 3rd ed., Vol. 5, pp. 267–290, by T. M. Hare, North Carolina State University; "Mechanical Properties and Behavior" under "Ceramics", in *ECT* 4th ed., Vol. 5, pp. 634–658, by Jill Glass, Sandia National Laboratories; "Ceramics, Mechanical Properties and Behavior," in *ECT* (online), posting date: December 4, 2000, by Jill Glass, Sandia National Laboratories.

CITED PUBLICATIONS

1. F. L. Riley, *J. Am. Ceram. Soc.* **83**(2), 245 (2000).
2. J. Wolf, ed., *Aerospace Structural Metals Handbook*. Battelle Metals and Ceramics Information Center, Columbus, Ohio, 1988.
3. D. J. Green, *An Introduction to the Mechanical Properties of Ceramics*, Cambridge University Press, Cambridge, 1998.
4. N. K. Sinha, *J. Mater. Sci.* **21**(5), 1533 (1986).
5. A. H. Cottrell, *The Mechanical Properties of Matter*, Robert E. Krieger Publishing Co., Huntington, New York, 1981.
6. O. Vardar, I. Finnie, D. R. Biswas, and R. M. Fulrath, *Int. J. Fract.* **13**(2), 215 (1977).
7. B. R. Lawn, *Fracture of Brittle Solids*, 2nd ed., Cambridge University Press, Cambridge, U.K., 1993.
8. H. Tada, P. Paris, and G. Irwin, *The Stress Analysis of Cracks Handbook*, Del Research Corp., St. Louis, Mo., 1973.
9. ASTM C1161-02b, Standard Test Method for Flexural Strength of Advanced Ceramics at Ambient Temperature.
10. D. Connolly, A. C. Stockton, and T. C. O'Sullivan, *J. Am. Ceram. Soc.* **72**(5), 859 (1989).
11. G. Quinn, *J. Am. Ceram. Soc.* **73**(8), 2374 (1990).
12. R. W. Rice, in W. W. Kriegel and H. Palmour, III, eds., *Materials Science Research*, Vol. 5, Plenum Press, New York, 1971, pp. 195–229.
13. H. Kim and A. J. Moorhead, *J. Am. Ceram. Soc.* **73**(3), 694 (1990).
14. M. Srinivasan, in J. B. Wachtman, Jr., ed., *Treatise on Materials Science and Technology*, Vol. 29, Academic Press, Inc., New York, 1989, pp. 99–159.
15. K. Breder, T. Anderson, and K. Scholin, *J. Am. Ceram. Soc.* **73**(7), 2128 (1990).
16. J. Homeny and W. L. Vaughn, *J. Am. Ceram. Soc.* **73**(2), 394 (1990).
17. K. Noguchi, M. Fujita, T. Masaki, and M. Mizushina, *J. Am. Ceram. Soc.* **72**(7), 1305 (1989).
18. R. W. Davidge, *Mechanical Behaviour of Ceramics*, Cambridge University Press, Oxford, U.K., 1986.
19. ASTM C1239-00, Reporting Uniaxial Strength Data and Estimating Weibull Distribution Parameters for Advanced Ceramics.
20. G. R. Anstis, P. Chantikul, B. R. Lawn, and D. B. Marshall, *J. Am. Ceram. Soc.* **64**(9), 533 (1981).
21. M. F. Ashby and D. R. H. Jones, *Engineering Materials, An Introduction to their Properties and Applications*, Pergamon Press, Elmsford, N.Y., 1980.
22. Y.-M. Mai and B. R. Lawn, *Ann. Rev. Mater. Sci.* **16**, 415 (1986).
23. T. Fett and D. Munz, *J. Mater. Sci. Lett.* **9**, 1403 (1990).
24. D. J. Green, R. H. J. Hannink, and M. V. Swain, *Transformation Toughening of Ceramics*, CRC Press, Inc., Boca Raton, Fla., 1989.

25. E. C. Subbarao, in A. H. Heuer and L. W. Hobbs, eds., *Science and Technology of Zirconia, Advances in Ceramics*, Vol. 3, The American Ceramic Society, Inc., Columbus, Ohio, 1981.
26. K. T. Faber and A. G. Evans, *Acta Metall.* **31**(4), 565 (1983).
27. *Ibid.*, pp. 577–578.
28. H. Liu, K. L. Weisskopf, and G. Petzow, *J. Am. Ceram. Soc.* **72**(4), 559 (1989).
29. L. M. Sheppard, *Ceram. Bull.* **71**(4), 617 (1992).
30. R. J. Kerans, R. S. Hay, N. J. Pagano, and T. A. Parthasarathy, *Ceram. Bull.* **68**(2) (1989).
31. M. S. Newkirk, *Ceram. Eng. Sci. Proc.* **8**(7–8), 879 (1987).
32. F. F. Lange, B. V. Velamakanni, and A. G. Evans, *J. Am. Ceram. Soc.* **73**(2), 388 (1990).
33. B. D. Flinn, F. W. Zok, F. F. Lange, and A. G. Evans, *Mat. Sci. Eng.* **A144**, 143 (1991).
34. G. V. Srinivasan, J.-F. Jue, S.-Y. Kuo, and A. V. Virkar, *J. Am. Ceram. Soc.* **72**(11), 2098 (1989).
35. A. V. Virkar and R. L. K. Matsumoto, *J. Am. Ceram. Soc.* **69**(10), C-224 (1986).
36. J. F. Jue and A. V. Virkar, *J. Am. Ceram. Soc.* **73**(12), 3650 (1990).
37. I.-W. Chen and L. A. Xue, *J. Am. Ceram. Soc.* **73**, 2585 (1990).
38. J. Poirier, *Creep of Crystals*, Cambridge University Press, New York, 1985.
39. W. D. Kingery, H. K. Bowen, and D. R. Uhlmann, *Introduction to Ceramics*, John Wiley & Sons, Inc., New York, 1976.
40. W. R. Cannon and T. G. Langdon, *J. Mater. Sci.* **18**, 1 (1983).
41. H. J. Frost and M. F. Ashby, *Deformation Mechanism Maps*, Pergamon Press, New York, 1982.
42. D. W. Richerson, *Modern Ceramic Engineering: Properties, Processing and Use in Design*, 2nd ed., Marcel Dekker, Inc., New York, 1992.
43. ASTM E384-99 Standard Test Method for Microhardness of Materials; ASTM C1327-99 Standard Test Method for Vickers Indentation Hardness of Advanced Ceramics.
44. C. P. Alpert, H. M. Chan, S. J. Bennison, and B. R. Lawn, *J. Am. Ceram. Soc.* **71**(8), C-371 (1988).
45. D. Sherman and D. Brandon, in R. Riedel, ed., *Handbook of Ceramic Hard Materials*, Wiley-VCH, 2000, pp. 66–103.
46. B. R. Lawn and R. J. Blau, eds., *Microindentation Techniques in Materials Science and Engineering*, International Metallographic Society, ASTM STP 889, 1986.
47. K. M. Liang, R. Torrecillas, G. Orange, and G. Fantozzi, *J. Mater. Sci. Lett.* **25**, 5077 (1990).
48. T. A. Michalske and B. C. Bunker, *Sci. Am.* **255**(12), 122 (1987).
49. C. Preece, ed., *Treatise on Materials Science and Technology*, Vol. 16, Erosion, Academic Press, Inc., New York, 1979.
50. A. M. Rajendran and W. H. Cook, *Joint report between the University of Dayton Research and the Air Force Armament Laboratory*, AFATL-TR-88-143 SBI-AD-E801 843, Dec. 1988, 99 pp.
51. R. J. Hand and J. E. Field, *Eng. Fract. Mech.* **37**(2), 293 (1990).
52. D. H. Buckley and K. Miyoshi, in Ref. 14, pp. 293–365.
53. D. B. Marshall and W. C. Oliver, *J. Am. Ceram. Soc.* **70**(8), 542 (1987).
54. T. E. Fischer, M. P. Anderson, and S. Jahanmir, *J. Am. Ceram. Soc.* **72**(2), 252 (1989).
55. E. K. Beauchamp and S. N. Burchett, in S. J. Schneider, Jr., ed., *Engineered Materials Handbook*, Vol. 4, *Ceramics and Glasses*, ASM International, 1991, pp. 532–541.
56. D. P. H. Hasselman, *Bull. Am. Ceram. Soc.* **49**(12), 1033 (1970).
57. G. A. Schneider and G. Petzow, *J. Am. Ceram. Soc.* **74**(1), 98 (1991).
58. J. Tsai, C. Yu, and D. K. Shetty, *J. Am. Ceram. Soc.* **73**(10), 2992 (1990).

59. L. Ewart and S. Suresh, *J. Mater. Sci.* **22**(4), 1173 (1987).
60. M. J. Reece and F. Guiu, *J. Am. Ceram. Soc.* **73**(4), 1004 (1990).
61. V. D. Fréchette, *Failure Analysis of Brittle Materials, Advances in Ceramics*, Vol. 28, The American Ceramic Society, Inc., Westerville, Ohio, 1990.
62. V. D. Fréchette and J. R. Varner, eds., *Advances in Ceramics*, Vol. 22, The American Ceramic Society, Inc., Westerville, Ohio, 1988.
63. J. J. Mecholsky, Jr., S. W. Freiman, and R. W. Rice, *J. Mater. Sci.* **11**, 1310 (1976).
64. ASTM C1322-02, Standard Practice for Fractography and Characterization of Fracture Origins in Advanced Ceramics.

S. JILL GLASS
Sandia National Laboratories
RAJAN TANDON
Sandia National Laboratories